Coupling between proton pseudo-spins and normal modes in ferroelectric glycinium phosphite

J. Agostinho Moreira* and A. Almeida
Departamento de Física, IFIMUP, Faculdade de Ciências da Universidade do Porto, Rua do Campo Alegre, 687, 4169-007 Porto, Portugal

L. G. Vieira and J. L. Ribeiro
Departamento de Física, Universidade do Minho, 4710-057 Braga, Portugal

M. R. Chaves and M. L. Santos
Departamento de Física, IFIMUP, Faculdade de Ciências da Universidade do Porto, Rua do Campo Alegre, 687, 4169-007 Porto, Portugal

A. Klöpperpieper
Fachbereich Physik, Universität des Saarlandes, 66041 Saarbrücken, Germany
(Received 21 December 2004; revised manuscript received 22 July 2005; published 21 September 2005)

This work reports a study of the temperature dependence (290–20 K) of the lattice dynamics of glycinium phosphite obtained from polarized Raman spectroscopy $[X(yy)Z]$ and infrared reflectivity $[\vec{E}\|\vec{b}]$ measurements. The loss of the inversion center at the para-ferroelectric phase transition gives rise to the activation of additional infrared and Raman bands. The oscillator strength of some infrared lattice modes that arise in the ferroelectric phase can be correlated with the temperature dependence of the order parameter of the phase transition. Several anomalies, which have been detected in the temperature dependence of the frequency and of the damping coefficient of some external and internal modes of the phosphite group, are described by a theoretical model that takes into account the coupling between proton pseudo-spins and phonons. The results obtained indicate that the phosphite group behavior affects the characteristic time of the proton flipping motion and reflects the long range ferroelectric order in glycinium phosphite.

DOI: 10.1103/PhysRevB.72.094111 PACS number(s): 77.84.−s, 63.20.−e, 78.30.−j, 64.60.−i

I. INTRODUCTION

Glycinium phosphite, $H_3NCH_2COO\cdot H_3PO_3$ (hereafter designated by GPI) is an adduct of glycine aminoacid and phosphorous acid. At room temperature, GPI crystallizes in the space group $P2_1/a$ and the unit cell contains four molecules.[1] Its structure consists of hydrogen bonded long chains of phosphite groups oriented parallel to the crystallographic c axis. The glycinium cation alternately attaches to the phosphite group by one hydrogen bond between one oxygen of its carboxylic groups and one phosphite oxygen. The amine group of glycinium cation is also hydrogen bonded to three different phosphite groups. Figure 1 shows a plot of the unit cell of GPI.

In the paraelectric phase, the hydrogen bonds between the carboxylic groups and the phosphite groups are relatively large (2.598 Å) and the protons in the interphosphite hydrogen chains are disordered over two different equilibrium positions.[1,2] In the ferroelectric phase, which occurs below $T_c=225$ K, these protons become statistically ordered.[1] Consequently, the glide plane perpendicular to the monoclinic b axis is lost and the space group in the ferroelectric phase becomes $P2_1$. The spontaneous ferroelectric polarization, directed along the monoclinic b axis, is perpendicular to the phosphite chains.[1,3] This contrasts with the situation found in the similar compound betainium phosphite (BPI), where the polarization is oriented parallel to those chains.[4] Moreover, the value of the saturated spontaneous polarization in GPI,[3] $P_s\approx 5\times 10^{-3}$ C/m^2, is lower than the corresponding value to the BPI,[4] $P_s\approx 17\times 10^{-3}$ C/m^2, and its critical exponent β $\{P_S\propto[(T_c-T)/T_c]^{\beta}\}$ is very close to $\beta=0.25$, a value that corresponds to a tricritical phase transition.[5]

Baran *et al.*[6,7] have shown that the dielectric relaxation in GPI (and in its deuterated analog DGPI) can be described in terms of a soft relaxational mode in the microwave frequency range. Contrary to the case of BPI, this mode may not be strictly associated with the proton flipping motion in a double potential well.[6] In fact, the value of the activation energy that has been estimated from the study of dielectric dispersion[6] ($\Delta U=17$ kJ mol^{-1}) is more than three times higher than the corresponding value in BPI (Ref. 8) ($\Delta U=5$ kJ mol^{-1}) and the macroscopic relaxation time[6] ($\tau=4\times 10^{-10}$ s near T_c) is about one order of magnitude longer[8] ($\tau=6\times 10^{-11}$ s for BPI). Therefore, the mechanism of the para-ferroelectric phase transition may not be solely determined by the movements of the protons in the interphosphite hydrogen bonds.

Proton nuclear magnetic resonance (NMR) measurements[9] and preliminary vibrational studies carried out on powdered samples of GPI (Refs. 6 and 10) have been interpreted by assuming that the ordering of the interphosphite protons is triggered by the rotation of the glycinium molecule about its long axis. This rotation would induce the ordering of protons along the inorganic anionic chain. However, recent neutron scattering investigations[11] did not confirm this key role of the organic molecular group in the

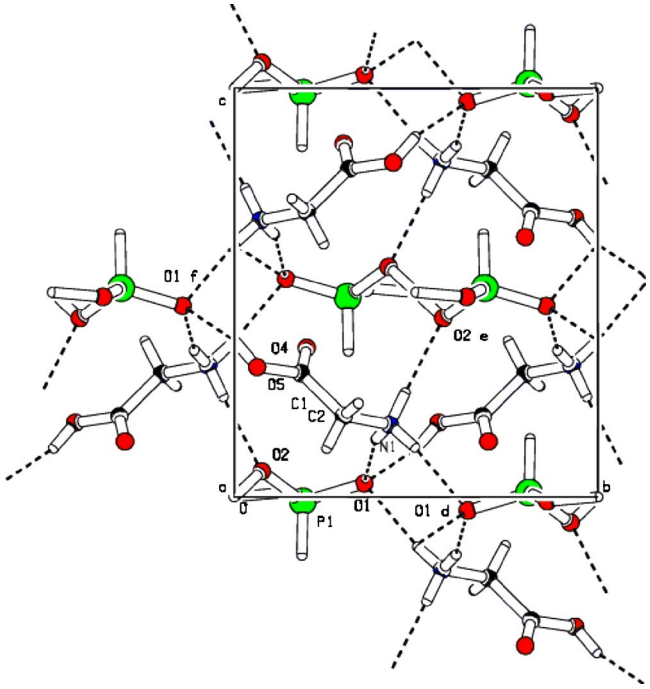

FIG. 1. (Color online) Unit cell of GPI at room temperature.

mechanism related to the phase transition. In fact, the ordering of the CH_2 group, expected to occur at T_c, has not been detected. On the other hand, the elastic neutron scattering data provided a clear evidence for the appearance of structural modifications in the phosphite group at the ferroelectric phase, which appears distorted with respect to its location and shape in the paraelectric phase.[11]

The aim of the present work is to help elucidate the role of the different molecular degrees of freedom in the onset of the ferroelectric phase of GPI. For this purpose, we focused our attention on the lattice dynamics and we analyzed the temperature dependence of the different normal modes across the phase transition. In order to identify the molecular degrees of freedom associated to each mode and to search for possible effects of coupling between normal modes and proton pseudo-spins, we have used the very detailed assignment of modes carried out by Sledz and Baran (Ref. 12) along with other literature data (Refs. 13 and 14).

We have only chosen to study the polarized infrared reflectivity ($\vec{E}\|\vec{b}$) at normal incidence and Raman spectra $X(yy)Z$, with $y\|b$ axis. This choice was made to avoid the complications that arise from the effect of the optical birefringence and dispersion of the principal dielectric axes. (Because the directions of two principal dielectric axes on the monoclinic plane may vary with frequency and temperature, the usual methods for the analysis of the dispersion cannot be directly applied.) In fact, under these experimental conditions (normal incidence and the electric field $\vec{E}$ of the incident wave oriented along the sole principal dielectric axis dictated by symmetry), the electromagnetic wave inside the crystal keeps the same polarization as the incident wave. This allows us to use conventional and much simpler methods to analyze infrared dispersion and Raman spectra. In addition, because the phase transition in GPI is caused by a relaxational soft mode with A_u symmetry,[6] we may expect that the effect of coupling between the order parameter and the lattice, should be more evident in the peculiarities of the temperature dependence of A_g $[X(yy)Z]$ and A_u $[\vec{E}\|\vec{b}]$ phonons.

II. EXPERIMENTAL DETAILS AND DATA ANALYSIS

The samples under study have been cut from one high quality single crystal, grown from aqueous solution by a technique of controlled solvent evaporation.

The polarized Raman spectra were registered with a Jobin-Yvon T64000 spectrometer equipped with a charge coupled device (CCD) camera (40–4000 cm^{-1}) and a photocounting device (10–200 cm^{-1}). The 514.5 nm line of an Ar^+ laser was chosen for excitation. The samples were cut in a rectangular parallelepipedic shape, with dimensions of $3\times4\times5$ mm^3 and optically polished faces oriented perpendicularly to the $x\|a^*$, $y\|b$, and $z\|c$ axes. The spectra were recorded in a right-angle scattering geometry $[X(yy)Z$, being $y\|b$ axis] over the spectral and temperature ranges of 10–4000 cm^{-1} and 20–300 K, respectively. Experimental conditions such as laser power, slit width, and acquisition time per spectrum were maintained constant for all the spectra taken. The spectral resolution was of the order of 1.5 cm^{-1}. The temperature stability during each measurement was better than ±0.2 K. The Raman spectra were simulated with a sum of N damped oscillators

$$I(\omega,T)=[1+n(\omega,T)]\sum_{j=1}^{N}A_{oj}\frac{\omega\Omega_{oj}^2\Gamma_{oj}}{(\Omega_{oj}^2-\omega^2)^2+(\omega\Gamma_{oj})^2}. \quad (1)$$

Here, $I(\omega,T)$ is the intensity of the scattered beam, $n(\omega,T)$ the Bose-Einstein factor; A_{oj}, Ω_{oj}, and Γ_{oj} the strength, frequency, and damping factor of the jth damped oscillator, respectively. At the low frequency range, the Rayleigh scattering was modeled by a Gaussian component with a temperature independent halfwidth of about 3.5 cm^{-1}.

Infrared (IR) reflectivity measurements were performed with a Bruker IFS 66V spectrometer. Room temperature pyroelectric detectors of DTGS with PE or KBr windows and Mylar 6μ-M8 or KBr beam splitters were used to cover the spectral range 40–4000 cm^{-1}. The spectral resolution was better than 4 cm^{-1}. The complex dielectric function has been evaluated from the IR data both by Kramers-Kronig inversion and by fitting the factorized form of the dielectric function[15]

$$\varepsilon(\omega)=\varepsilon_\infty\prod_{j=1}^{N}\frac{\Omega_{jLO}^2-\omega^2-i\omega\Gamma_{jLO}}{\Omega_{jTO}^2-\omega^2-i\omega\Gamma_{jTO}}, \quad (2)$$

to the reflectivity spectra at normal incidence, via

$$R(\omega)=\left|\frac{\sqrt{\varepsilon(\omega)}-1}{\sqrt{\varepsilon(\omega)}+1}\right|. \quad (3)$$

In Eq. (2), $\Omega_{jTO(LO)}$ and $\Gamma_{jTO(LO)}$ represent the frequency and damping coefficient of the jth transversal (longitudinal)

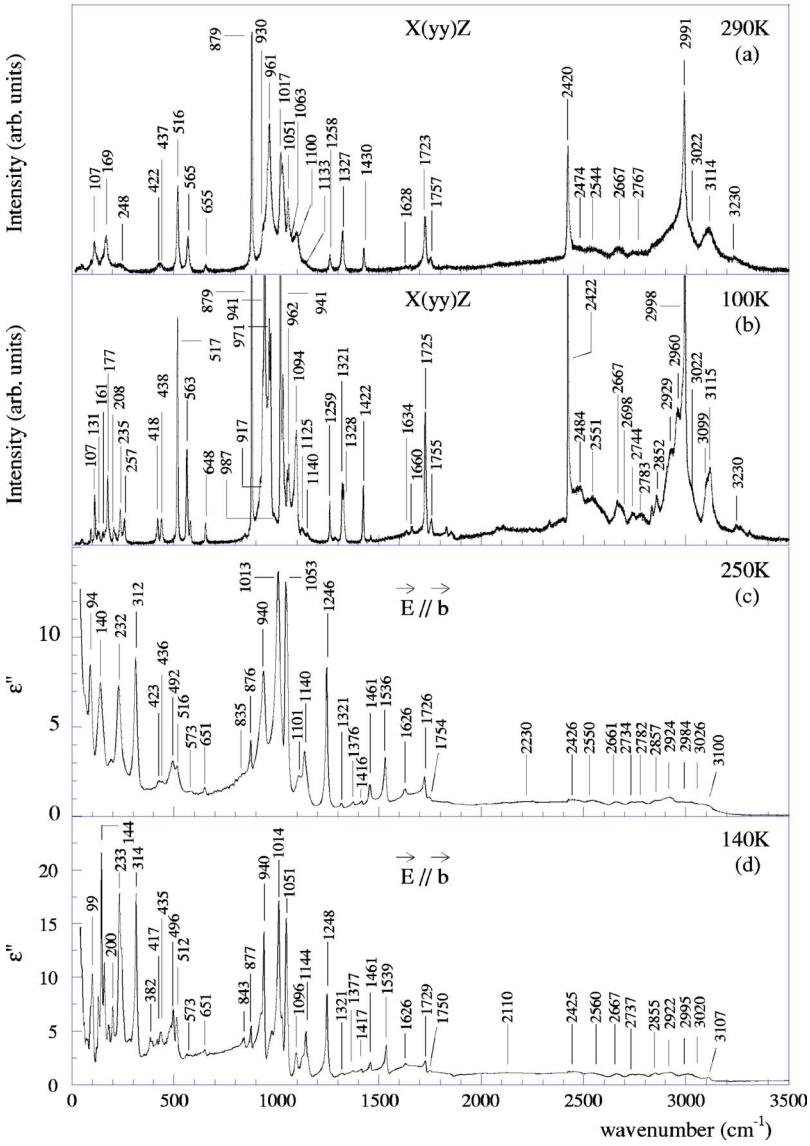

FIG. 2. (Color online) Vibrational spectra of GPI. From top to bottom: $X(yy)Z$ Raman spectra recorded at 290 (a) and 100 K (b); the spectra of the imaginary part of the dielectric constant calculated by the Kramers-Kronig transformation of the $\vec{E}\|\vec{b}$ polarized infrared reflectivity spectra recorded at 250 K (c) and at 140 K (d). The wave numbers corresponding to the more relevant bands detected in each phase are displayed.

optical mode, and ε_∞ the electronic contribution to the dielectric constant. From the fitting, the oscillator strength $\Delta\varepsilon_j$ of each mode can be evaluated as

$$\Delta\varepsilon_j = \frac{\varepsilon_\infty}{\Omega_{jTO}^2} \frac{\prod_{k=1}^{N} (\Omega_{kLO}^2 - \Omega_{jTO}^2)}{\prod_{k\neq j}^{N} (\Omega_{kTO}^2 - \Omega_{jTO}^2)}. \quad (4)$$

Due to the difficulties raised by the complexity of the spectra and by the many overlapping reflectivity bands, we have imposed the condition of equal damping coefficients for longitudinal and transversal optical modes ($\Gamma_{jLO}=\Gamma_{jTO}$). Under such a condition, the factorized form (2) corresponds to the conventional sum of polar Lorentz oscillators.

In general, the ε'' spectra obtained from the reflectivity by Kramers-Kronig inversion and by the fitting the factorized form of the dielectric function are found in good agreement. However, the fitting procedure allows us to estimate more accurately the values of the transversal and longitudinal wave numbers of the different optical modes, along their oscillator strength and the damping coefficients.

III. EXPERIMENTAL RESULTS

Figure 2 shows the $X(yy)Z$ Raman spectra [Figs. 2(a) and 2(b)] and the imaginary part of the dielectric constant ε'' [Figs. 2(c) and 2(d)] obtained above and below $T_c=225$ K. The dielectric loss ε'' shown in this figure was calculated from Kramers-Kronig inversion of the reflectivity spectra. The wave numbers corresponding to the more relevant bands detected at each phase are also displayed.

As referred to above, the unit cell of GPI contains four formula units, each one containing 17 atoms. In the paraelectric phase, the factor group of the unit cell is isomorphic to the point group $2/m$. Among these 68 atoms, 64 occupy general positions and four special positions of symmetry $\bar{1}$ (the protons in the interphosphite hydrogen bonds). Consequently, the factor group analysis gives the following decom-

position for the 204 normal vibrations at the Γ point of the Brillouin zone

$$\Gamma^{\text{total}} = [(A_u + 2B_u)_{\text{acus}} + (12A_g + 12B_g + 11A_u + 10B_u)_{\text{opt}}]_{\text{ext}} + (36A_g + 36B_g + 42A_u + 42B_u)_{\text{opt,int}}.$$

In the paraelectric phase, we could therefore expect to detect 53 A_u (IR active) and 48A_g (Raman active) modes. Below T_c, due to the loss of the glide plane, these two sets of modes should become visible both in the $X(yy)Z$ Raman and $(\vec{E}\|\vec{b})$ infrared spectra, giving a total of 101 detectable modes.

However, the differences observed in the spectra taken at the paraelectric and ferroelectric phases are not very dramatic. In spectra of complex molecular crystals such as GPI, this may partially result from the fact that some of the bands may overlap with others and remain unresolved or be too weak to be detected. But another reason must be considered in order-disorder transitions, where a soft relaxational mode related to proton flipping motion in a double potential well plays the central role. In such a case, if the protons motion has relatively long flipping characteristic times, the instantaneous crystal structure detected by Raman and IR spectroscopies may correspond to a symmetry that is effectively lower than that detected by x ray. This is clearly the case with GPI, where the fundamental ferroelectric dispersion appears in microwave frequency range.[4]

We have studied in detail the temperature dependence of the spectra and evaluated the parameters characterizing the various vibrational modes by simulating the spectra with the model forms described in the previous section. In the following, we will present the most relevant modifications detected across the phase transition in the infrared and Raman spectra.

A. Temperature dependence of the IR spectra

Figure 3 shows the frequency dependence of the imaginary part of the dielectric function, $\varepsilon''(T)$, in the spectral ranges of 30–400 cm^{-1} [Fig. 3(a)] and 800–1300 cm^{-1} [Fig. 3(b)] for several temperatures between 140 and 250 K. The functions $\varepsilon''(T)$ shown were calculated from the fitting procedure previously described. Table I summarizes the values of the parameters fitted to the spectra taken at 250 and 140 K. Outside the spectral ranges depicted in Fig. 3, we could not detect any significant changes in the reflectivity spectra.

In the frequency range of the external modes [$\omega < 300$ cm^{-1}; see Fig. 3(a)], one can observe the rise of at least four bands that are either absent or are very weak in the paraelectric phase. At $T=140$ K, these bands are located at 90, 118, 242, and 278 cm^{-1} [see arrows in Fig. 3(a)]. The oscillator strengths $\Delta\varepsilon$ of these bands were calculated from Eq. (4). As an illustrative example, let us consider the temperature dependence of the strength of the lattice mode located at 242 cm^{-1} (value at 140 K), shown in Fig. 4. In the ferroelectric phase, the value of $\Delta\varepsilon(T)$ increases significantly as the temperature decreases from $T_c=225$ K. The solid line presented in Fig. 4 represents the best fit of the equation

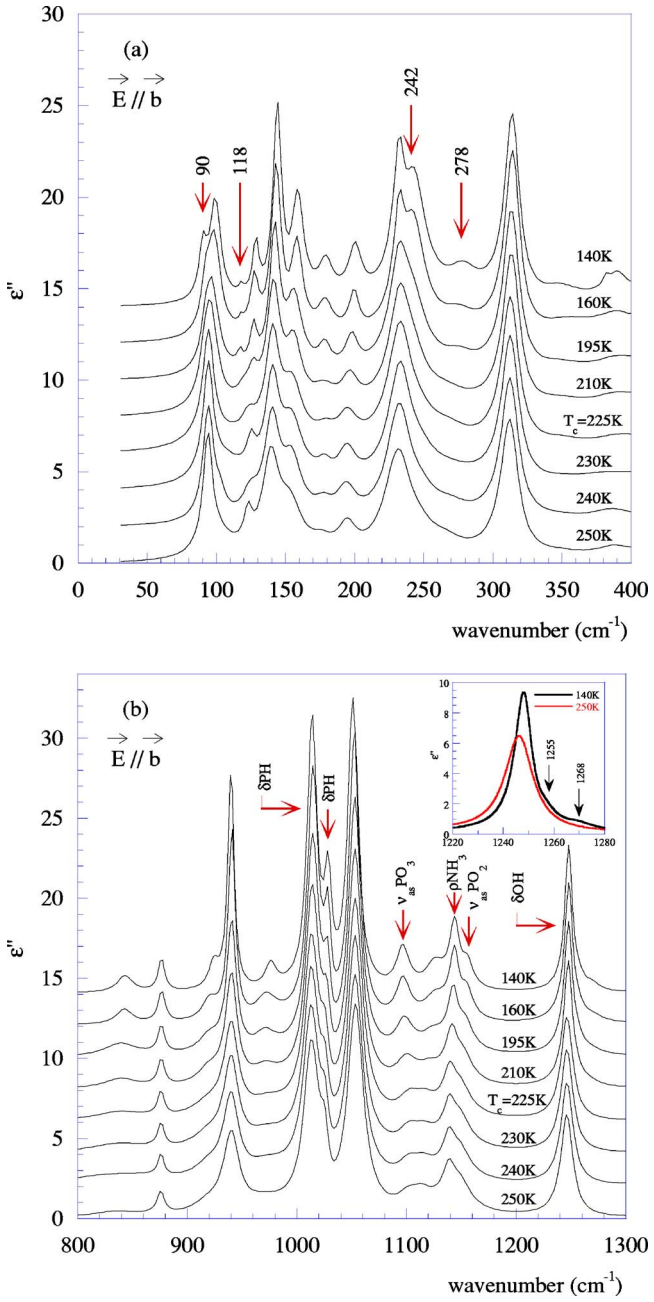

FIG. 3. (Color online) Spectra of the imaginary part of the dielectric constant calculated from the fitting of the factorized model [Eq. (2)] to the $\vec{E}\|\vec{b}$ infrared reflectivity spectra, for several temperatures, in the spectral range (a) 30–400 and (b) 800–1300 cm^{-1}. Inset Fig. 3(b): spectra of the imaginary part of the dielectric constant in the range 1220–1280 cm^{-1}, taken at 250 and 140 K. The arrows indicate the new bands visible below T_c (values at 140 K).

$$\Delta\varepsilon(T) = A\left(\frac{T_c - T}{T_c}\right)^{\beta} \propto P_S(T), \tag{5}$$

to the $\Delta\varepsilon(T)$ values, with $\beta=0.25$ as a fixed parameter. In fact, this value of the β exponent was checked from the temperature dependence of the spontaneous polarization, obtained from the integration of the pyroelectric current (see inset in Fig. 4). As can be seen, within the experimental

TABLE I. Values of the parameters fitted to the infrared reflectivity spectra recorded at 250 and 140 K.

$T=140$ K				$T=250$ K			
Ω_{TO} (cm^{-1})	$\Gamma_{TO}=\Gamma_{LO}$ (cm^{-1})	Ω_{LO} (cm^{-1})	$\Delta\varepsilon$ (cm^{-2})	Ω_{TO} (cm^{-1})	$\Gamma_{TO}=\Gamma_{LO}$ (cm^{-1})	Ω_{LO} (cm^{-1})	$\Delta\varepsilon$ (cm^{-2})
90	7	91	0.194	94	8	97	0.529
99	9	102	0.505	102	20	104	0.192
118	4	118	0.014	123	7	124	0.090
129	5	129	0.113	140	15	144	0.523
144	7	148	0.509	153	21	159	0.326
159	10	164	0.341	195	16	197	0.108
179	12	181	0.129	232	23	242	0.531
200	11	203	0.144	265	29	268	0.066
233	9	235	0.263	312	15	327	0.355
242	20	256	0.532	344	62	348	0.048
278	25	282	0.120	388	30	391	0.037
314	13	329	0.403	423	30	425	0.038
348	33	352	0.063	436	9	436	0.009
382	5	383	0.007	466	64	470	0.072
390	19	393	0.060	492	19	495	0.051
417	9	418	0.020	516	34	526	0.104
435	35	444	0.173	573	80	577	0.029
477	35	485	0.150	651	11	652	0.006
496	9	500	0.045	835	50	836	0.017
512	15	523	0.087	876	8	877	0.012
573	80	577	0.028	918	31	919	0.018
651	15	652	0.008	940	17	947	0.084
843	18	845	0.021	969	43	971	0.029
877	7	878	0.016	1013	16	1022	0.146
924	11	925	0.018	1026	8	1030	0.019
940	7	948	0.098	1053	18	1086	0.205
976	12	977	0.018	1101	22	1104	0.015
1014	11	1022	0.170	1113	25	1120	0.022
1029	8	1033	0.043	1140	12	1142	0.026
1051	11	1082	0.193	1146	24	1169	0.039
1096	14	1107	0.034	1246	13	1269	0.066
1125	20	1131	0.026	1321	14	1322	0.003
1144	10	1151	0.035	1376	14	1377	0.002
1155	13	1171	0.019	1416	8	1416	0.001
1248	8	1255	0.066	1461	14	1463	0.009
1255	11	1265	0.006	1536	11	1541	0.021
1268	14	1276	0.004	1660	190	1689	0.097
1321	17	1323	0.004	1726	11	1729	0.006
1377	17	1378	0.005	1754	32	1759	0.009
1417	14	1418	0.004	1834	173	1849	0.033
1461	12	1463	0.009	2014	90	2016	0.006
1539	10	1545	0.025	2098	397	2107	0.025
1676	195	1717	0.148	2111	92	2113	0.002
1729	12	1733	0.004	2230	219	2245	0.032
1750	11	1751	0.002	2426	208	2442	0.033
1803	150	1821	0.034	2550	144	2562	0.020
2013	157	2023	0.024	2661	45	2664	0.004

TABLE I. (*Continued.*)

$T=140$ K				$T=250$ K			
Ω_{TO} (cm^{-1})	$\Gamma_{TO}=\Gamma_{LO}$ (cm^{-1})	Ω_{LO} (cm^{-1})	$\Delta\varepsilon$ (cm^{-2})	Ω_{TO} (cm^{-1})	$\Gamma_{TO}=\Gamma_{LO}$ (cm^{-1})	Ω_{LO} (cm^{-1})	$\Delta\varepsilon$ (cm^{-2})
2105	100	2109	0.015	2734	78	2738	0.007
2110	115	2113	0.001	2782	52	2785	0.004
2230	199	2247	0.037	2857	92	2864	0.011
2425	211	2451	0.051	2924	71	2933	0.014
2560	107	2572	0.017	2984	45	2986	0.002
2667	47	2671	0.007	3026	85	3035	0.012
2737	57	2740	0.006	3100	85	3109	0.010
2783	56	2787	0.007				
2855	59	2859	0.008				
2922	79	2935	0.019				
2995	53	2998	0.005				
3030	67	3040	0.012				
3107	64	3113	0.007				
$\varepsilon\infty=2.58$				$\varepsilon\infty=2.52$			

accuracy of the measurement, the increase of $\Delta\varepsilon(T)$ with decreasing temperature correlates well with the temperature dependence of the spontaneous polarization $P_S(T)$.

In the frequency range 350–650 cm^{-1}, where the bands associated to the bending modes of the PO_3 groups are found,[12] we could not observe significant spectral modifications apart from the normal sharpening of the bands caused by the decrease in temperature. On the other hand [see Fig. 3(b)], the ordering of interphosphite hydrogen bonds seems to contribute to sharpen and alter the frequency of the bands originating from the PO_3 stretching mode ($\nu_{as}PO_3$; 1101 cm^{-1}) and the bending mode of the P-H bond (δPH; 1013 and 1026 cm^{-1}). As shown in Fig. 5, the temperature dependence of several mode frequencies in the spectral range 1010–1150 cm^{-1} reflects the phase transition related to the ordering of protons. Not unexpectedly, some of these bands are related to internal modes of the PO_3 group, directly linked to the oxygen atoms O1 and O2, to which the protons are bonded (see Fig. 1). In the frequency range 1240–1270 cm^{-1} [see Figs. 3(b) and 5] we have observed a

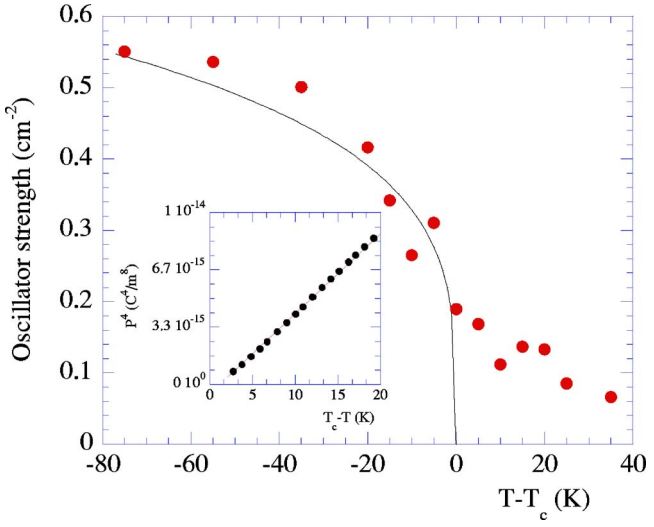

FIG. 4. (Color online) Temperature dependence of the oscillator strength $\Delta\varepsilon(T)$ the lattice mode located at 242 cm^{-1} (value at 140 K) in the $\vec{E}\|\vec{b}$ infrared reflectivity spectra (dots). The solid line represents the best fit of the equation $\Delta\varepsilon(T)=A[(T_c-T)/T_c]^{\beta}$, with $\beta=0.25$, to the $\Delta\varepsilon(T)$ values. Inset: temperature dependence of the fourth power of the spontaneous polarization, obtained from the integration of the pyroelectric current.

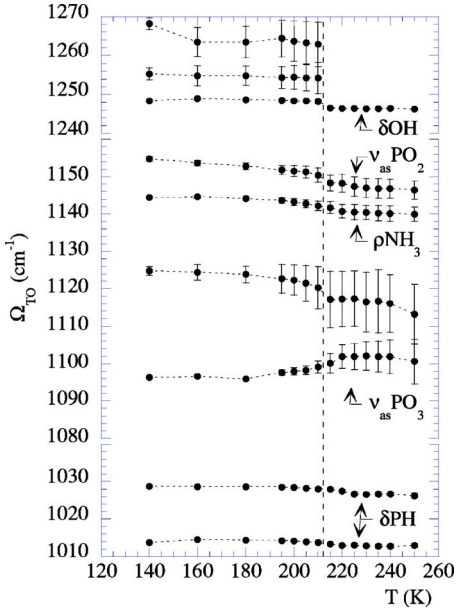

FIG. 5. (Color online) Temperature dependence of the transverse optical frequency of the internal modes, observed in the $\vec{E}\|\vec{b}$ infrared reflectivity spectra, in the spectral range of 1010–1270 cm^{-1}.

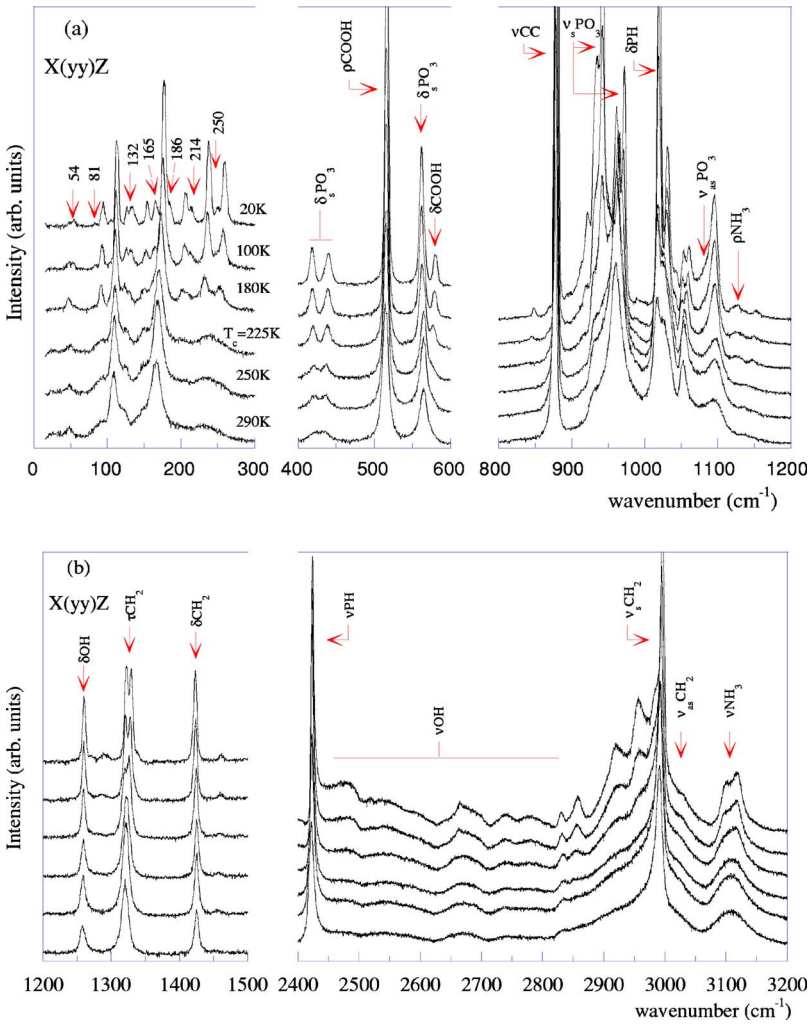

FIG. 6. (Color online) Raman spectra recorded in the $X(yy)Z$ scattering geometry, for several temperatures, in the spectral range: (a) 20–300; 400–600; 800–1200 cm^{-1} and (b) 1200–1500; 2400–3200 cm^{-1}.

small anomaly at T_c in the temperature dependence of the wave number of the δOH mode, together with the appearance of two bands. These latter bands are located, at 140 K, at 1255 and 1268 cm^{-1}, as the temperature is lowered below T_c. These bands can be better seen in the inset of Fig. 3(b), where the spectra of the imaginary part of the dielectric constant, taken at 250 and 140 K, are shown in the appropriate frequency range. These bands correspond very likely to the infrared activation of δOH modes of the hydrogen bonds.

Between 1300 and 1800 cm^{-1}, a visual inspection of the observed bands reveals no relevant changes as the temperature decreases below T_c. In particular, some internal modes of the glycinium unit, such as the $\nu C{=}O$, δCH_2, δNH_3 modes, do not show any clear critical behavior. Similarly, the parameters of the diffuse reflectivity bands that are located in the spectral range 2000–3400 cm^{-1} and ascribed to the P-H, O-H, CH_2, and NH_3 stretching modes, do not display also, any significant modifications across the phase transition. In particular, we could not detect in the IR spectra any drastic change of the CH_2 asymmetric stretching band located at about 3026 cm^{-1}.

A last remark concerns the possible occurrence of a second phase transition at low temperatures, as it has been suggested in Ref. 6 from the analysis of infrared transmission data measured on powdered samples. In this work, the authors reported the observation of important modifications of the transmission spectra taken at 15 K and conjecture a possible occurrence of an additional low temperature phase transition in GPI. In order to confirm this hypothesis, we have measured the reflectivity spectrum down to 15 K. Aside from the normal sharpening and better definition of the bands due to the temperature decreasing, the lower temperature reflectivity spectrum does not exhibit any peculiarity compared to the one taken at $T=140$ K. At least from the results obtained for this particular polarization, we cannot corroborate the existence of the proposed phase transition in GPI.

B. Temperature dependence of Raman spectra

Figure 6 shows the temperature dependence of the $X(yy)Z$ Raman spectra observed in the frequency ranges of 15–1200 cm^{-1} [Fig. 6(a)], 1200–1500 and 2400–3200 cm^{-1} [Fig. 6(b)]. Figure 7 depicts the temperature dependence of the wave number of the Raman bands observed in these spectral ranges, along with the temperature dependence of the damping coefficient of some selected modes.

In the frequency range of the lattice modes [15–300 cm^{-1}, see Fig. 7(a)], one can observe the appearance of seven additional bands on entering the ferroelectric phase. These

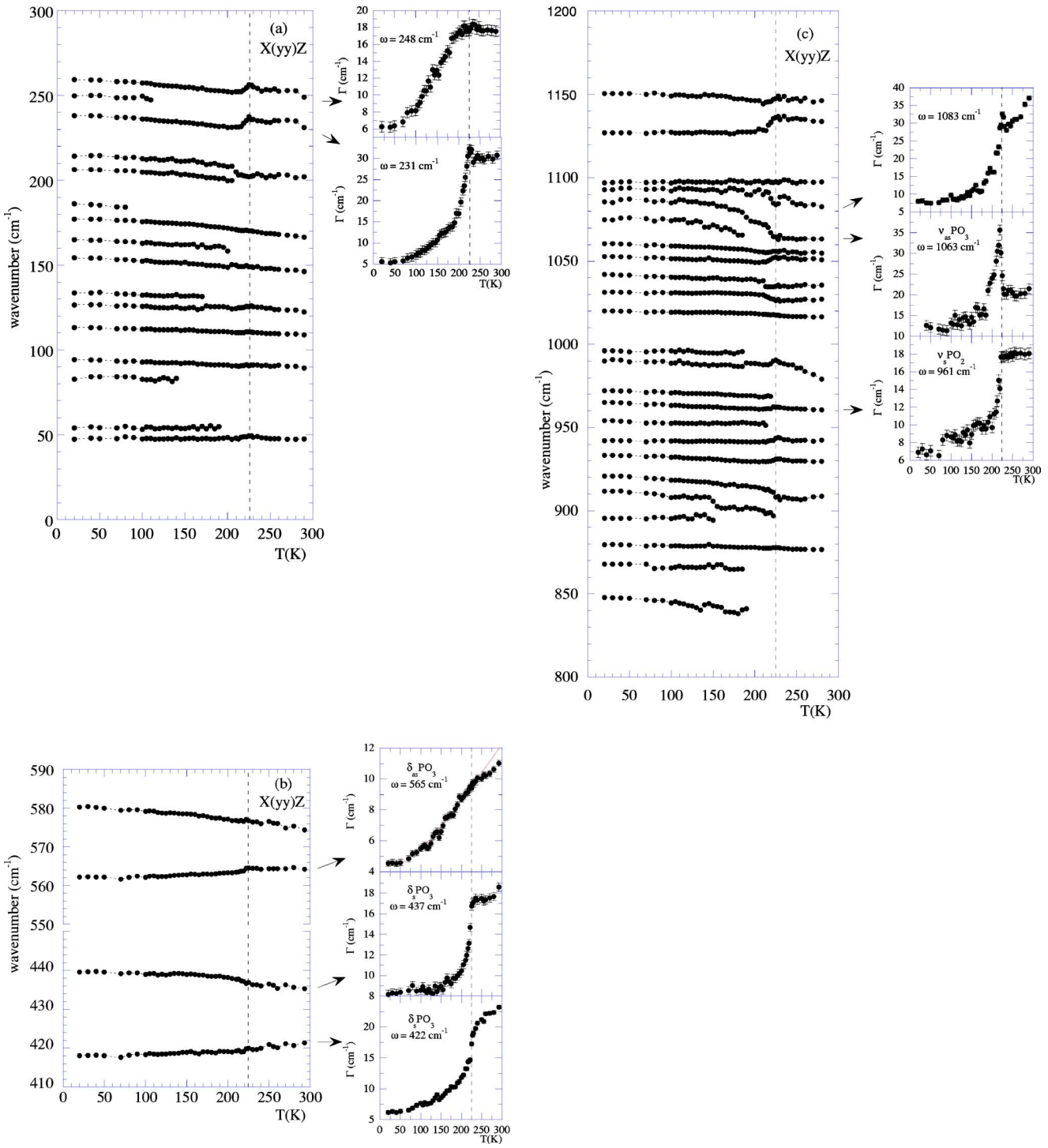

FIG. 7. (Color online) Temperature dependence of the wave number and bandwidth coefficient of the Raman bands observed in the spectral range: (a) 20–300; (b) 400–600; and (c) 800–1200 cm^{-1}.

bands, which can be better identified in Fig. 7(a), are likely to originate from external modes that are IR active in the paraelectric phase (A_u modes) and become Raman active as a result of the symmetry breaking at T_c. In addition, the bandwidth coefficients (Γ) of some external A_g modes display a marked critical behavior. This observation is illustrated in the insets in Fig. 7(a), where $\Gamma(T)$ corresponding to the modes located at 231 and 248 cm^{-1} is shown.

In the spectral region 400–600 cm^{-1} [see Fig. 6(a)], we can observe the bending modes $\delta_s PO_3$ (422 cm^{-1};437 cm^{-1}) and $\delta_a PO_3$ (565 cm^{-1}) along with the rocking mode ρCOOH (518 cm^{-1}) and the bending mode δ COOH (574 cm^{-1}). Among these, only the modes related to the phosphite tetrahedron display critical anomalies in the temperature dependence of their wave numbers and bandwidths [see Fig. 7(b)].

At higher frequencies [800–1200 cm^{-1}, Figs. 6(b) and 7(c)] the spectra are complex because of the overlap in frequency of several modes. Here, the phase transition noticeably affects both the intensities and bandwidths of several bands and gives rise to the splitting of some of them. These effects are particularly evident in the spectral range corresponding to the stretching modes of the PO_3 group ($\nu_s PO_2$; 930–975 cm^{-1}; $\nu_{as} PO_3$; 1063 cm^{-1}), to the in-plane vibration of the P-H bond (δPH; 1017 cm^{-1}) and to the rocking vibrations of NH_3 (ρNH_3; 1133 cm^{-1}).

We could detect several critical anomalies in the temperature dependence of both the wave number and bandwidth of some stretching modes of the PO_3 group [950–1150 cm^{-1}, Fig. 7(c)]. The wave number of the broadband located about 1063 cm^{-1} at room temperature, which has been assigned to the asymmetric stretching mode of the phosphite group, $\nu_{as} PO_3$, shows marked temperature dependence in the ferroelectric (FE) phase. As illustrated in the insets in Fig. 7(c), the temperature dependence of the bandwidths of some of these modes also displays interesting features. Due to the anharmonic terms in the vibrational potential energy,[16] the width of the Raman bands usually decreases by lowering the temperature. However, the widths of the bands related to the stretching PO_3 modes show marked anomalous temperature dependences near the phase transition.

Figure 6(b) illustrates the temperature dependence of the Raman spectra in the spectral ranges 1200–1500 and 2400–3200 cm^{-1}. Here we can identify some bands originating from internal vibrations of the glycinium cation; the twist mode τCH_2 (1327 cm^{-1}), the bending mode δCH_2 (1430 cm^{-1}), the stretching modes $\nu_s CH_2$ (2991 cm^{-1}) and $\nu_{as} CH_2$ (3022 cm^{-1}), and the stretching mode νNH_3 (3114 cm^{-1}), together with the diffuse bands due to the stretching of the O-H bond (νOH; 2600–2800 cm^{-1}). It can be seen that the bands related with the τCH_2 and νNH_3 vibrational modes split on entering into the ferroelectric phase.

The splitting of the Raman bands related to the CH_2 modes has been previously reported,[6,10] along with similar effects in modes related to the C=O stretching and COOH bending of the glycinium cation. To a great extent, this wealth of glycinium internal modes displaying a marked critical behavior, could suggest that the dynamics of the molecular organic group would play a key role in the mechanism of the phase transition.[6,10] However, we could not detect any relevant modification in the vibrational parameters related to the carboxyl group of glycine. The splitting of the bands related to the τCH_2 and to the νNH_3 modes is entirely consistent with structural data that disclose the appearance, below T_c, of two nonequivalent types of glycinium cations. So, this fact by itself does not allow us to conclude that the organic cation plays an active role in the phase transition.

IV. DISCUSSION AND CONCLUSION

The results described in the preceding section show that the observed modification in the vibrational spectra are more subtle than those we could expect just based on symmetry considerations. The modifications detected are essentially related to the activation of a number of additional external modes in the ferroelectric phase, to the behavior of the bands related to the τCH_2 and νNH_3 modes, and to the critical anomalies displayed by the vibrational parameters related to the phosphite group. The wave number, at room temperature, of the modes presenting a clear critical behavior is summarized in Table II.

TABLE II. Wave number (values at room temperature) of the bands observed in the $X(yy)Z$ Raman spectra and in the $\vec{E}\|\vec{b}$ infrared reflectivity spectra of GPI, whose temperature behavior shows clear critical anomalies. The mode assignment was based in Ref. 12.

$X(yy)Z$ (cm^{-1})	$\vec{E}\|\vec{b}$ (cm^{-1})	Assignment
231		Lattice mode
248		Lattice mode
422		$\delta_s PO_3$
437		$\delta_s PO_3$
565	564	$\delta_{as} PO_3$
909		
930		
942		$\nu_s PO_2$
961		$\nu_s PO_2$
978		
1017	1013	δ PH
	1026	δ PH
1051		νP=O or νCN
1063		$\nu_{as} PO_3$
1083		
1100	1101	$\nu_{as} PO_3$
1113	1113	
1133	1140	ρNH_3
1146	1146	$\nu_{as} PO_2$
	1246	δOH
1327		τCH_2
2991		$\nu_s CH_2$
3022		$\nu_{as} CH_2$
3114		νNH_3

The combined use of IR and Raman techniques allowed us to observe, below the phase transition, either the infrared or the Raman activation of several modes corresponding to distinct symmetries in the paraelectric phase (A_g and A_u, respectively). In the range of the external modes, we have shown that the intensity of the bands originated from A_g modes of the paraelectric phase is proportional to the order parameter $P_S(T)$.

In regard to the internal modes of the glycinium cation, we observed that the infrared spectra do not exhibit significant changes in their vibrational parameters. Contrasting with this fact, Raman data provide evidence for the splitting of the τCH_2 and νNH_3 bands. These results may indicate that the structural changes occurring at the phase transition can alter more significantly the polarizability of the CH_2 and NH_3 groups than their dipolar strengths. This interpretation

seems entirely consistent with the fact that both the bond length and angle of the organic cation remain essentially constant on crossing the phase transition.

Most of the anomalies detected in the temperature dependence of wave numbers and bandwidths are related to the phosphite group modes. This is not unexpected because the inorganic anions are bonded by the protons in the interphosphite hydrogen bonds. The parameters characterizing the bending and stretching modes of the inorganic group clearly reflect the phase transition, related to the ordering of the protons associated to its oxygen atoms O1 and O2. This is in agreement with neutron scattering results,[11] which show that the two nonequivalent sets of phosphite ions (here designated by ph1 and ph2, respectively) in the ferroelectric phase are slightly deformed with respect to their shape in the paraelectric phase. This deformation is mainly due to the shift of the position of O2 in ph2 (see Figs. 1 and 7 of Ref. 11) induced by the ordering of O2-H-O1 bond. Also, the length of the P-H bond was found to be reduced from 1.406 Å, above T_c, to 1.403 Å (ph1) or 1.400 Å (ph2). It is very likely that the reduction in bond length affects the frequency and damping coefficient of the P-H bending modes. Curiously, only the Raman data provided evidence for anomalies in the temperature dependence of the parameters of the bending modes $\delta_s PO_3$ (422 cm^{-1}; 437 cm^{-1}) and $\delta_a PO_3$ (565 cm^{-1}).

As we shall see, the observed critical behavior in the normal modes of the inorganic anion can be described by considering a model that accounts for the coupling between the proton pseudo-spins and the normal coordinates of the internal vibrations of the PO_3 group.

In fact, by following the lines of the model developed by Schaack and Winterfeldt for triglycine sulphate (TGS) and triglycine selenate (TGSe),[17] we are led to include in the Hamiltonian of the harmonic lattice a set of coupling terms expressed as a power expansion of the type

$$H_{S,L} = \sum_k U(k)Q(k)S(k) + \sum_{\vec{k},\vec{k}'} U(\vec{k},\vec{k}')Q(\vec{k})Q^*(\vec{k}+\vec{k}')S(\vec{k}') + \ldots . \quad (6)$$

Here, $Q(\vec{k})$ represents the normal coordinate of a given normal mode with the wave vector $\vec{k}$, $U(\vec{k})$ a coupling constant and $S(\vec{k})$ the Fourier transform of the z projection of the pseudo-spin operator σ_μ^z.

In order to account for anomalies, such as the frequency shifts induced from the nonharmonic terms in (6), we need to include terms that are at least quadratic in the normal mode coordinates. In such a case, the effect of the coupling terms is the renormalization of the phonon energies which, for $\vec{k}'=\vec{0}$ and replacing $S(\vec{0})$ by its thermal average $\langle S(\vec{0})\rangle = P_S(T)$, can be expressed as

$$\omega_{ph}^2(T,\vec{k}) = \omega_{ph}^2(T_c,\vec{k}) + 2U(\vec{k})P_S(T). \quad (7)$$

In GPI, the frequency shift disclosed in some bands at the para-ferroelectric phase transition may result from the change of some bonding energy in the poliatomic PO_3 group as a result of the ordering of the neighbor protons.

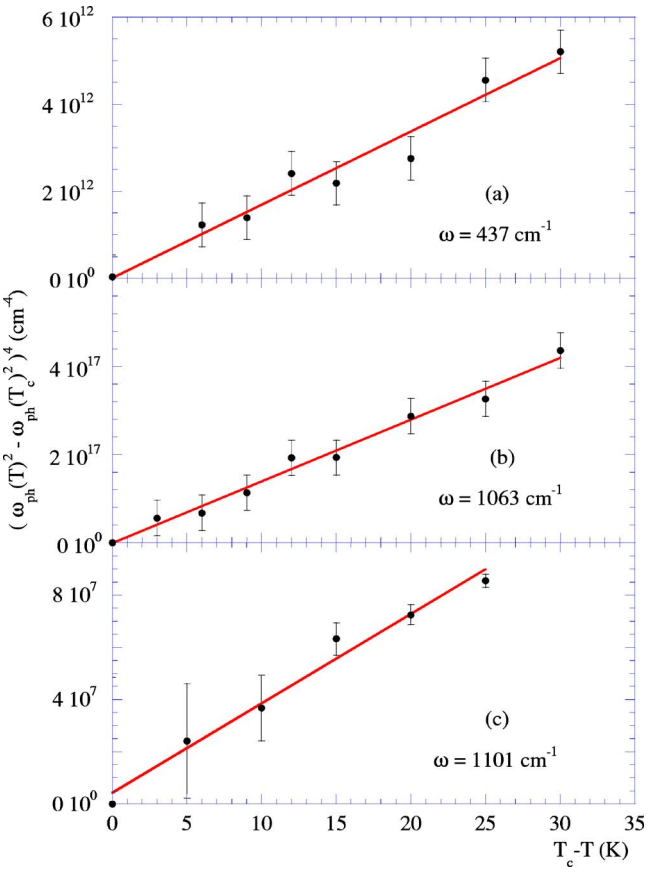

FIG. 8. (Color online) Temperature dependence of the fourth power of the shift of the squared frequency of internal modes of the phosphite anion observed in: (a) and (b) the $X(yy)Z$ scattering geometry, (c) in the $\vec{E}\|\vec{b}$ infrared reflectivity spectra. The solid lines represent the best fit of Eq. (8) to the data.

As referred to above, the critical exponent of the order parameter is $\beta=0.25$ (Ref. 5). Consequently, the fourth power of the shift of the squared phonon frequency must be a linear function of temperature

$$[\omega_{ph}^2(T) - \omega_{ph}^2(T_c)]^4 \propto T_c - T. \quad (8)$$

In agreement with this behavior (see Fig. 8), the fourth power of the shift of the squared frequency for three internal modes of the phosphite group varies linearly with temperature. The bands chosen correspond to the Raman modes detected near 437 and 1063 cm^{-1} [see Figs. 7(b) and 7(c)], along with the infrared mode detected near 1100 cm^{-1} (see also Fig. 5).

Let us now consider the effect of the nonharmonic terms in the bandwidth of a given mode. Because the critical broadening of the bandwidth (Γ) results from the energy fluctuations of the phonon modes, it must directly reflect the mean-square deviation of the frequencies:

$$\Gamma^2 \propto (\langle S^2(\vec{0})\rangle - \langle S(\vec{0})\rangle^2). \quad (9)$$

Hence, the critical temperature dependence of Γ is essentially determined by the Fourier component $\vec{k}=\vec{0}$ of the

pseudo-spin fluctuations. Note that, in accordance with this result, the $\Gamma(T)$ observed for some lattice modes and for several phosphite modes exhibits cusplike anomalies at T_c [see insets of Figs. 7(a) and 7(c)]. In particular, the damping coefficient $\Gamma(T)$ of the lattice mode near 231 cm^{-1} (room temperature value) and of the asymmetric stretching mode $\nu_{as}PO_3$, near 1063 cm^{-1} (room temperature value), exhibits a behavior that follows qualitatively the temperature dependence of the electric susceptibility, as expected from Eq. (9). This shows unambiguously that the critical behavior of these modes is a direct consequence of the critical behavior of the pseudo-spin fluctuations.

The temperature dependence of the oscillator strength of the infrared activated A_g mode, located at 242 cm^{-1} (value at 140 K), follows a law of proportionality with respect to the order parameter P_S, displaying in this way the increasing of the dipolar character of this lattice mode. The bands observed in the infrared and Raman spectra at 242 and at 252 cm^{-1} (values at 140 K), respectively, may correspond to the same mode. Taking into account the pronounced anomaly displayed by the wave number as a function of the temperature and the temperature dependence of the oscillator strength and of the damping coefficient, which reflect the coupling between the proton pseudo-spin and lattice vibration, it is reasonable to relate it with a lattice mode strongly coupled to the interphosphite hydrogen bonds.

The preceding considerations strongly suggest that the coupling between proton pseudo-spins and phosphite normal coordinates plays an important role in the phase transition of GPI. Such a coupling may help to explain why the absolute value of P_S in the state of saturation is smaller in comparison to other crystals of hydrogen bonded compounds and why the values of the activation energy and relaxation time in GPI differ from those expected for a mechanism strictly connected with the movements of the protons.

*Electronic address: jamoreir@fc.up.pt

[1] M. Th. Averbuch-Pouchot, Acta Crystallogr., Sect. C: Cryst. Struct. Commun. **49**, 815 (1993).
[2] F. S. Shikanai, M. Komukae, Z. Czapla, and T. Osaka, J. Phys. Soc. Jpn. **71**, 498 (2002).
[3] S. Dacko, Z. Czapla, J. Baran, and M. Drozd, Phys. Lett. A **223**, 217 (1996).
[4] J. Albers, A. Köpperpieper, H. J. Rother, and S. Haussühl, Ferroelectrics **81**, 27 (1988).
[5] R. Tchukvinskyi, R. Cach, Z. Czapla, and S. Dacko, Phys. Status Solidi A **165**, 309 (1998).
[6] J. Baran, G. Bator, R. Jakubas, and M. Sledz, J. Phys.: Condens. Matter **8**, 10647 (1996).
[7] J. Baran, M. Sledz, R. Jakubas, and G. Bator, Phys. Rev. B **55**, 169 (1997).
[8] G. Koch and H. Happ, Ann. Phys. (N.Y.) **2**, 522 (1993).
[9] J. Tritt-Goc, N. Pislewski, L. Szczepariska, and R. Goc, Solid State Commun. **108**, 189 (1998).
[10] T. Runka, M. Kozielski, M. Drozdowki, and L. Szczepariska, Ferroelectrics **239**, 995 (2000).
[11] H. Taniguchi, M. Machida, and N. Koyano, J. Phys. Soc. Jpn. **72**, 1111 (2003).
[12] M. Sledz and J. Baran, J. Mol. Struct. **706**, 15 (2004).
[13] M. L. Santos, A. Almeida, J. Agostinho Moreira, M. R. Chaves, A. Köpperpieper, and F. Gervais, J. Phys.: Condens. Matter **10**, 6147 (1998).
[14] P. Simon and F. Gervais, Phys. Rev. B **32**, 468 (1985).
[15] D. W. Berreman and F. C. Unterwald, Phys. Rev. **174**, 791 (1968).
[16] M. Balkanski, R. F. Wallis, and E. Haro, Phys. Rev. B **28**, 1928 (1983).
[17] G. Schaack and V. Winterfeldt, Ferroelectrics **15**, 35 (1977).